Organic Cation Dynamics in Hybrid Perovskite Device Performance

Henry de Vries
Zernike Institute for Advanced Materials,
University of Groninigen

(Research Paper NS190 - Guided by prof. dr. T.L.C. Jansen)
(Dated: March 20, 2016)

In the search for high-efficiency photovoltaics, hybrid perovskites of the form $APbI_3$ have generated broad attention with their reported high efficiencies. However, there is relatively little known about the relation between the dynamics of the organic cation A and the macroscopic charge transport properties that underlie the extraordinary device performance in hybrid perovskites. Taking $CH_3NH_3PbI_3$ as a case study, we present an overview of theoretical studies on how the dynamics of the methylammonium cation ($CH_3NH_3^+$) contribute to increased device performance. These mechanisms, comprised of dynamical band gap properties, unusual defect physics and ferroelectricity are critically assessed based on physical assumptions, computational limitations and a comparison with experimental results. We find that modeling of the atomistic origins of macroscopic properties call for a currently unavailable multi-scale approach, in order to improve consistency amongst theoretical predictions. Also, we find that experimental work denies a proposed significant influence of ferroelectricity on hybrid perovskite photovoltaic performance.

CONTENTS

INTRODUCTION

It goes without saying that the search for reliable, scalable and renewable high-performance photovoltaic devices is one of the key research themes in nanoscience, comprising efforts from a wide range of disciplines. In the past half decade, a revival of research interest in a class of materials called perovskites has taken place, due to its promising photovoltaic properties. Organic-inorganic hybrid perovskite photovoltaics $APbI_3$, with A

being a cation, have shown an increase in solar cell efficiency from below 4% (2009) towards 20% (2015).[1–4] Various physical properties of perovskite materials that support potential photovoltaic applications are the presence of a direct band gap, good (ambipolar) charge carrier mobilities and a low exciton binding energy resulting from the high dielectric screening ($\epsilon \approx 20-30$).[1,2,4–6] Besides desirable physical properties, the processibility of perovskites that has come with recent developments in solid-state chemistry and molecular electronics has contributed significantly to the reported efficiency increase, and allows for potential large-scale production of perovskite photovoltaics.[1,2,5,7]

Whereas the recent developments with regards to device efficiency and processibility are outstanding, there are various hurdles that have to be overcome in order for hybrid perovskite photovoltaics to be implemented as a technology. One of these hurdles consists of gaining an understanding of the role of the organic cation component of hybrid perovskites. Both theoretical and experimental works have thus far not resulted in fully identifying the relation between the dynamics of the organic cation and the charge transport properties of hybrid perovskite photovoltaics. Clarifying this relation will allow for better modeling of device behavior, resulting in possible improvements in the design of devices. This might benefit perovskite photovoltaic technology as a whole.

In this paper, we will therefore assess recent theoretical findings with respect to the relation between cation dynamics and hybrid perovskite performance, focusing on the hybrid halide perovskite $CH_3NH_3PbI_3$. We introduce various structural principles of commonly used hybrid perovskites and discuss the most commonly used theoretical and experimental methods which are used to study perovskite properties. Next, we provide an overview of proposed physical mechanisms underlying the relation between cation dynamics and hybrid perovskite device performance.[3,7,8] This discussion is divided into a treatise based on the dynamics of the methylammonium cation ($CH_3NH_3^+$) in the perovskite $CH_3NH_3PbI_3$. The various consequences of the cation dynamics that will be discussed consist of dynamical bandgap properties, macroscopical phenomena such as ferroelectricity and the bulk photovoltaic effect, and unusual defect physics. Ultimately, we critically assess the validity of recent theoretical insights by considering i) computational limitations and the quality of the underlying physical assumptions in simulation, ii) the relation between real crystal structures and the ones assumed in theoretical methods, and iii) a comparison between theoretical predictions and recent experimental work, in which we discuss specifically findings regarding ferroelectricity.

1. HYBRID PEROVSKITE STRUCTURES AND BASIC PROPERTIES

1.1. Crystal structure and phases

Starting from the most general perovskite structural formula ABX_3, we can define a unit cell, consisting of five atoms, in which cation A has 12 nearest neighbours and cation B is located in BX_6 octahedra. The crystal structure and unit cell for ABX_3 are depicted in Fig. 1.

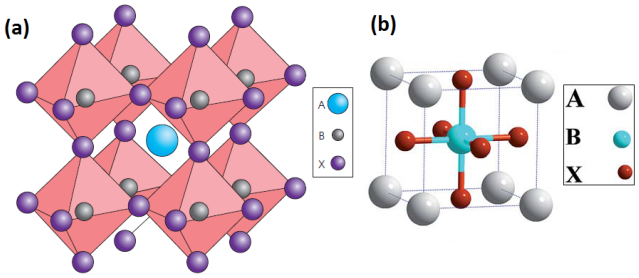

FIG. 1. General ABX_3 perovskite crystal structure (a) and unit cell (b) in the α-phase. The cation A is in this review taken to be the methylammonium cation $CH_3NH_3^+$. B is in general Pb, with X being a halide (I or Cl). Note that whereas both images contain spherically symmetric cations A, this does not have to be the case for all structures. Images adapted from refs. 3 and 4.

In order for the perovskite structure to be stable, certain ratios between the ionic radii of A,B and X should be obeyed. In general, this analysis is done via the tolerance

factor[3] t, which is defined as:

$$t = \frac{(R_A + R_X)}{\sqrt{2}(R_B + R_X)}, \quad (1)$$

in which R_A, R_B, R_X are the ionic radii of the corresponding ions A, B and X. When $t \approx 1$ does not hold, the perovskite structure is distorted, which implies $R_A >> R_B$. When relatively large Pb- and I atoms are used at the B- and X sites respectively, we directly see that a large cation A is a necessary to keep t close to 1 and the perovskite crystal stabilized. Organic cations are therefore often chosen. Examples consist of ammonium (NH_4^+), methylammonium ($CH_3NH_3^+$) or formamidinium ($H{=}NCHNH_3^+$).[2,3,9] Considering the choices for B and X fixed, variation of A will influence the crystal symmetry and stability. The undistorted crystal structure at $t \approx 1$ is cubic and denoted as the α-phase. Lowering of t yields a subsequent tetragonal β-phase and an orthorhombic γ-phase.[3,10] Besides the β- and γ-phases, breaking of the B-X bond might occur, resulting in a completely different δ-phase.[3,10] As the conditions under which the δ-phase occurs are not present during perovskite device operation, we will not discuss this phase further in this review. Transitions between the α, β and γ phases, which show a decreasing amount of cation disorder, can be induced by factors such as electric field, temperature and pressure.[3,7] It is specifically worth mentioning that the room-temperature phase of $CH_3NH_3PbI_3$ is the β-phase. An overview of the lattice constants and symmetry groups for the α,β and γ-phases is given in Table I.

When we treat any kind of crystal structure, it should, however, be clear that real crystals cannot easily be assumed 'perfect'. Added to the general notion of imperfect crystal structures, we should note that the mesoporous TiO_2-$CH_3NH_3PbI_3$ structure that is often used in perovskite devices is hard to characterize.[3] Recent X-ray diffraction measurements proved that besides the well-known(α,β,γ,δ) structures, a lower-order symmetry is present in real hybrid perovskite materials[7,14]. As a whole, the $CH_3NH_3PbI_3$ is highly disordered at ambient conditions, with a local, lower symmetry structure the size of about 2 α-phase lattice constants (in each direction) being present. This corresponds to a grain size of approximately 1.4 nm[3,14]. In conventional polycrystalline materials, the presence of grain boundaries can influence optical properties[14].

TABLE I. Overview of structural properties of $CH_3NH_3PbI_3$ for the α-, β- and γ-phases. Lattice constants are given as theoretical value and experimental values, respectively. Table, including theoretical values adapted from refs. 3 and 11

Phase	Symmetry	Lattice constants (Å)
α	$Pm\bar{3}m$	a = 6.39 / 6.28[12]
β	$I4/mcm$	a= 8.80/8.85[13] c=12.99/12.64[10,12]
γ	$Pbnm$	a = 8.84/8.56[12] b = 8.77/8.56[12] c = 12.97/12.58[12]

1.2. Electric and optical properties

For a subsequent discussion of the relation between cation dynamics and perovskite device performance, knowledge of the electrical and optical perovskite properties is necessary. The most distinctive feature between fully inorganic and hybrid perovskites is the asymmetry of the cation.

The asymmetric and therefore dipolar methylammonium cation ($CH_3NH_3^+$) is present in the center of the $CH_3NH_3PbI_3$ perovskite cage and has a dipole moment of 2.3 Debye.[7] The presence of the methylammonium cation gives rise to a polarization of the perovskite, allowing for a dielectric response. In devices, this means that a dielectric response ϵ_0 consists of the sum of a fast electronic and a slow ionic polarization.[7]

The electronic structure of $CH_3NH_3PbI_3$ is dominated by the I 5p and Pb 6s orbital character of the upper valence band maximum (VBM), with the Pb 6p orbitals comprising the conduction band minimum (CBM). From

this, we note two things. First is that this band structure is effectively the inverse of the conventional semiconductor band structure, which usually has s-orbitals dominating the conduction band minimum and p-orbitals dominating the valence band minimum.[3,15] Second is that the effect of the organic cation on the perovskite band structure can assumed to be small, or at least indirect.[3,7,15–17] From a band structure point of view, the main contribution of the cation is to stabilize the perovskite cage via the requirement $t \approx 1$, with the inorganic perovskite cage determining the band structure. Variation of the cation between Cs^+, to $CH_3NH_3PbI_3^+$ to $N{=}NCHNH3^+$ show band gap variation due to a change in lattice constant, without the presence of a clear trend.[3,18,19] A result of the perovskite band structure is the effective charge carrier mass m^*, which is obtained via the curvature of the energy dispersion of the respective valence and conduction bands for holes and electrons[3,20]:

$$m^* = \hbar^2 \left[\frac{\partial^2 \epsilon(k)}{\partial k^2} \right]^{-1}. \tag{2}$$

where $\epsilon(k)$ is the energy dispersion and k the wave vector. Based on the presence of lone-pair s electrons on the Pb atoms, an unconventional situation in perovskites exists in comparison to conventional semiconductors. The cation Pb p orbitals, comprising the conduction band, are significantly higher in energy than the anion p orbitals, leading to a strongly dispersive $CH_3NH_3PbI_3$ conduction. However, strong $s-p$ coupling around the VBM results into the upper valence band of $CH_3NH_3PbI_3$ also being dispersive. Following this argument, the electron- and hole effective masses in perovskites were found to be very comparable (0.35 resp. 0.31), meaning that perovskite devices are ambipolar in nature.[3,15,20] We can explain this effect by considering the fact that charge carrier mobility scales inversely with the effective charge carrier mass. Assuming a comparable scattering time for both types of charge carriers, we find that a perovskite device should be capable of operating using both electrons and holes as charge carriers.[20]

Besides the presence of ambipolar charge carrier properties, a key factor in perovskite solar cell performance is the high optical absorption. Reported efficiencies of 15% have been achieved with absorber layers below a thickness of 500 nm, which largely consists of scaffold (supporting TiO_2/SiO_2 nanostructures) layers.[3,21,22] Two factors need to be considered in order to fundamentally describe the absorption of a material. These are the transition matrix elements between the states in the valence- and conduction bands, and the joint density of states (JDOS) between the two. Effectively, we can see that the optical absorption depends on both the product between the probability of optical transitions and the density of available transitions. An overview of the (joint-)density of states and absorption spectra is given in Fig. 2 for a conventional, direct-band gap semiconductor (GaAs) and the typical hybrid perovskite $CH_3NH_3PbI_3$.

We can explain the significant differences (1 order of magnitude) between (hybrid) perovskite and conventional semiconductor (GaAs) absorption by considering their respective transition dynamics and JDOS.[3,15] In GaAs, absorption occurs via a direct intra-atomic transition between As p orbitals and As s orbitals, or interatomically between As p and Ga s orbitals. The perovskite absorption transition is also direct in nature, but consists of transitions between I p to Pb p orbitals (interatomic), or Pb s to Pb p orbitals (intra-atomic). The difference in absorption strength resides in the higher conduction band DOS in perovskites, leading to a higher JDOS. Also, the intra-atomic transitions in $CH_3NH_3PbI_3$ have much higher probabilities than the inter-atomic transitions in GaAs.[3,23] An comparison is given between electronic properties of GaAs and $CH_3NH_3PbI_3$ is given in Table II.

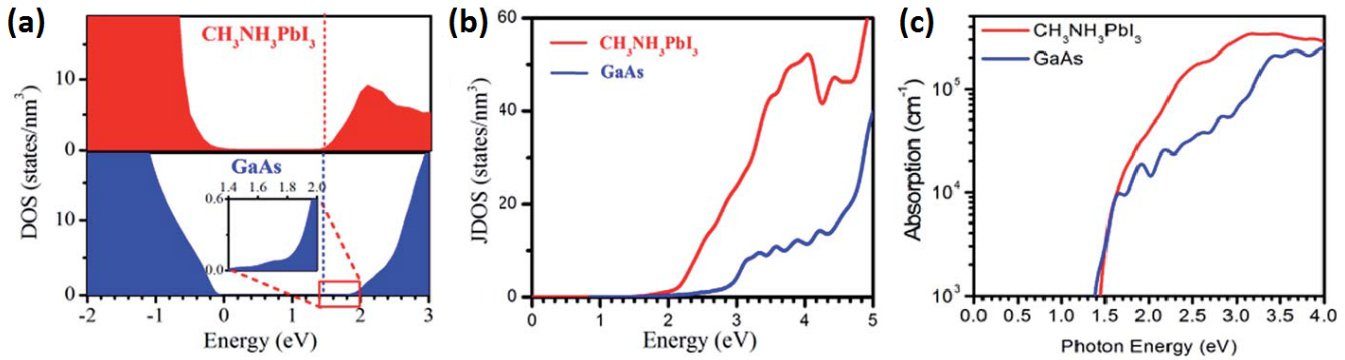

FIG. 2. Comparison of optical properties between GaAs and $CH_3NH_3PbI_3$. (a) Density of states, rescaled such that the valence band maxima coincide with 0 energy. Dashed lines indicate the corresponding conduction band minima. (b) Comparison of the different JDOS. Note the significant difference between perovskite and conventional absorbers due to band structure inversion and dispersion as mentioned in section 1.2. (c) Logarithmic absorption spectra, showing the significant difference in absorption in the visible region (1.7-3.2 eV). Image adapted from ref 15.

TABLE II. Comparison between GaAs and $CH_3NH_3PbI_3$ electronic properties, consisting of effective charge carrier masses, band gap energy and CBM and VBM characteristics. Note that the values for $CH_3NH_3PbI_3$ are for the β-phase. Data taken from refs 3, 4, and 15.

	m_e^*	m_h^*	E_g (eV)	CBM	VBM
$CH_3NH_3PbI_3$	$0.35m_e$	$0.31m_e$	1.57/1.52	Pb $6p$	I $5p$, Pb $6s$
GaAs	$0.07m_e$	$0.34m_e$	1.43	Ga s, As s	As p

2. EXPERIMENTAL AND THEORETICAL METHODS

To investigate the relation between cation dynamics and hybrid perovskite performance, an appreciable understanding of both the commonly used theoretical- and experimental methods is necessary. In this section we will introduce the state-of-the-art in *ab initio* molecular dynamics approaches, and shortly discuss more macroscopic models. We will also provide an overview of the various experimental methods in use, and their resolutions with respect to unraveling organic cation dynamics in hybrid perovskites.

2.1. Theoretical methods

The starting point for modeling the effects of organic cation dynamics on perovskite device performance consists of molecular dynamics (MD) calculations. Typically, the heart of MD calculations consists of accurately modeling the interactions between the atoms in a structure. The corresponding (original) approach is therefore to take interatomic potentials as a pre-calculated input, and proceed iteratively, while calculating the (electronic) influence on nuclear position in every iteration.[24] Various properties of condensed phase systems are then found from the time evolution (read: dynamics) of the atoms. However, purely MD calculations prove no value for 'chemically complex' situations, such as electronic band structures and covalent bonding. For describing these properties, density functional theory (DFT) is performed. In DFT, the many electron Schrödinger equation is solved iteratively. The starting point is to reduce the many-body problem to a single-body problem[24]. This is acheived by using Kohn-Sham formalism,[25] in which an electron density $n(\mathbf{r}) = \sum_i |\phi_i(\mathbf{r})|^2$ is introduced as a key variable, with $\phi_i(\mathbf{r})$ being occupied single-particle orthonormal orbitals. This method, however, performs poorly with regards to exchange interactions and is computationally costly. Also, there are no dynamics involved in the use of DFT. For example, calculations of electronic

structures are made under the assumption of stationary atomic nuclei. *De facto*, DFT is therefore performed at an effective temperature of 0 K.

Nowadays, *ab initio* methods involving an efficient combination of both MD and DFT are used, which in general are based on the Car-Parrinello approach.[24,26,27] Meaning 'from first principles', *ab initio* models compute the forces acting on the nuclei from electronic structure (DFT) calculations. This occurs while the trajectory from MD is still generated, treating the electronic variables as active degrees of freedom, instead of fully calculating many electron solutions of the Schrödinger equation per iteration. The Car-Parrinello approach specifically achieves this by coupling nuclear- and electronic motion into two equations of motion via an extended Lagrangian[26]:

$$M_I \ddot{\mathbf{R}}_I = -\nabla_I E\big[\{\phi_i\}, \{\mathbf{R}_J\}\big] \tag{3}$$

$$\mu \ddot{\phi}_i(\mathbf{r}, t) = -\frac{\delta E}{\delta \phi_i^*(\mathbf{r}, t)} + \sum_j \Lambda_{ij} \phi_j(\mathbf{r}, t). \tag{4}$$

In the nuclear equation of motion (eq. 3), $E\big[\{\phi_i\}, \{\mathbf{R}_J\}\big]$ is the Kohn-Sham energy density functional, generating energy values as a function of Kohn-Sham orbitals and nuclear position. In the electronic equation of motion, E retains its meaning, and Λ_{ij} denotes a Lagrangian multiplier matrix. When considering the interplay between cation dynamics and perovskite photovoltaic performance, it is important to realise the limitations of Car-Parrinello-based *ab initio* MD approaches. Whereas powerful, combinations of MD and DFT are also very computationally demanding, requiring vast amounts of assumptions.[24] Examples[28] are the use of small amounts of unit cells (<100 atoms in total), periodic boundary conditions and short simulation times (<100 ps). These computational limitations, together with the implications of various simplifying assumptions will be discussed more elaborately in section 4.

2.2. Experimental methods

Determining the orientation of the organic cation in hybrid perovskites is challenging, and is greatly complicated by temperature-induced disorder and the fact that time-resolved techniques are often necessary to gain an understanding of the cation dynamics. Here, we shortly introduce three key techniques that are in use for determining the dynamical properties of the organic cation in perovskites. Also, an overview of the relevant time-resolutions of the discussed techniques is given in Table III.

First attempts at elucidating the dynamics of the methylammonium cation in $CH_3NH_3PbI_3$ were made using NMR spectroscopy.[5] Typically, spin-lattice relaxation times are measured using inversion recovery, which is based upon subsequently applying 180 degrees (inversion) and 90 degrees (transverse) RF waves. Following the temperature dependence of the spin-lattice relaxation times, correlation times for the dynamics of the perovskite cation can be obtained.[29] Alternatively, quasielastic neutron scattering (QENS) is capable of directly measuring the orientation of the methylammonium cation in $CH_3NH_3PbI_3$ on the ps- to ns time scale.[30] A schematic description of neutron scattering on the methylammonium cation is depicted in Fig. 3. QENS works on the premise that the cross section for incoherent scattering on hydrogen atoms (as present on the ends of the methylammonium cation) is an order of magnitude greater than the other elements in $CH_3NH_3PbI_3$.[30,31] This allows for probing the dynamics of the methylammonium cation instead of the inorganic perovskite cage components. Spectra are recorded for various $\mathbf{Q}$ at different temperatures. Lorentzians can be fitted for all spectra, with the fitting parameters carrying information on the nature of methylammonium cation motion in perovskites.[30]

In the late 90's, two-dimensional infrared spectroscopy (2DIR) came in use, as a short-timescale alternative to

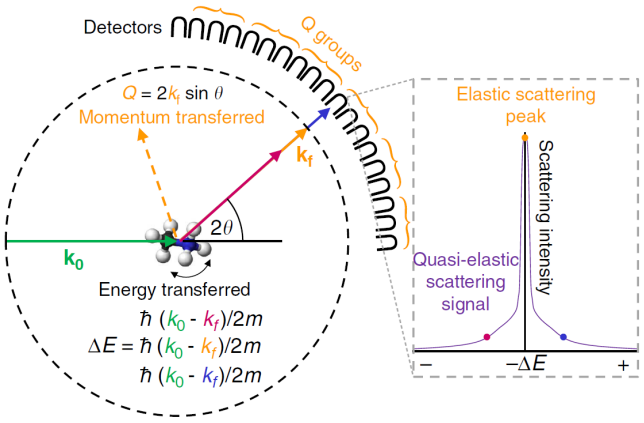

FIG. 3. Setup for QNES. Incoming neutrons carry a momentum $\mathbf{k_0}$ and transfer a momentum $\mathbf{Q} = 2\mathbf{k_f}\sin\theta$ to the methylammonium ion, with k_f being the backscattered neutron momentum and 2θ the scattering angle. Typical spectra are displayed to the right of the setup, and are averaged in groups of detectors, denoted Q groups. Image adapted from ref. 30

NMR.[32,33] In 2DIR, vibrational modes are excited using an interferometric pair of femtosecond-scale IR pulses.[5,34] Then, the system is allowed to evolve for a certain waiting time, after which a probe pulse is applied. The time-resolved absorption, as measured via the probe pulse, allow for finding the time domain in which the dynamics of the probed cation take place. The probe pulses are often also split into parallel and perpendicular orientations with respect to the pump excitation pulses. This allows for measuring the time-dependent transmission changes for both polarizations. From the polarization changes and their corresponding time dependencies (also called anisotropy), information can be obtained on the degree in which the transition dipoles in the probed medium are coupled. The decay of the polarizational anisotropy occurs allows one follow dynamics in real-time. To determine whether intra-molecular relaxation occurs, or that the decay is due to certain re-orientations of the transition dipoles themselves, a theoretical treatment is necessary.[5,32,33]

The benefit of 2DIR consist of the capability of interpreting the time dependence of various peaks in IR spectra, which allows to identify dynamics that occur on different timescales. Advances in spectroscopy, optics and computational methods for calculating correlations have allowed for processes to be studied on the femtosecond scale, providing a much better time resolution than NMR or QNES.[34]

3. CATION DYNAMICS AND PEROVSKITE DEVICE PERFORMANCE

3.1. Cation orientation: what do we know?

We center the discussion on the interplay between cation dynamics and perovskite device performance on the spherically asymmetric methylammonium cation(MA, $CH_3NH_3^+$). As was mentioned in section 1.2, the starting points are that the methylammonium cation has a permanent dipole due to its asymmetry, and has a structurally stabilizing role in the perovskite cage due to its size.[3–5,10,15]

In section 1.1, the various phases of perovskite structures were discussed. There is a strong correlation between the various structural symmetries of the inorganic perovskite cage and the resulting electronic properties, as expressed via the electronic band structure discussed in section 1.2. One important aspect of the according distortions of the perovskite cage, is its relation to the rotational freedom (or lack thereof) of the methylammonium cation.

Recent findings from 2D-IR spectroscopy,[5] based on earlier work in NMR[29] and QENS[30], together with corresponding MD simulations[5] have provided a clearer view on the rotational dynamics of the methylammonium cation in $CH_3NH_3PbI_3$. As of now, two clearly distinct rotational modes were identified as a cone-shaped wobbling on a sub-picosecond timescale, and large angle jumps (90°) occurring at the scale of several picoseconds.

TABLE III. Overview of experimental methods used for measuring methylammonium cation dynamics, including time resolution. Also depicted are the proposed cation dynamics with corresponding timescales, as suggested by various experimental methods.

Method	Time resolution	Proposed cation dynamics (time scale)
NMR	10^{-1}ps[29]	high-temperature disorder (ps)[29]
QENS	ps-ns[30,31]	dynamic reorientation (14 ps)[30]
2D IR	fs[5,32,34]	Cone-shaped wobbling (0.3 ps),[5] dynamic reorientation (ps)[5]

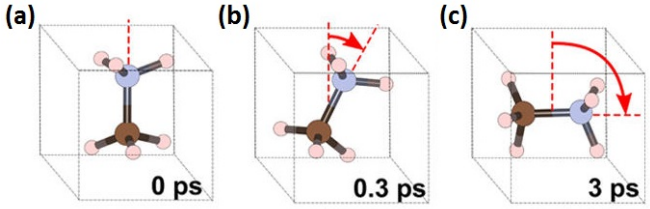

FIG. 4. Overview of the two rotational modes of the methylammonium ion in $CH_3NH_3PbI_3$. (a) Default position. (b) Cone-shaped vibration with respect to the crystal axis. (c) reorientation of methylammonium with respect to $CH_3NH_3PbI_3$ iodine atoms. Image adapted from ref. 5

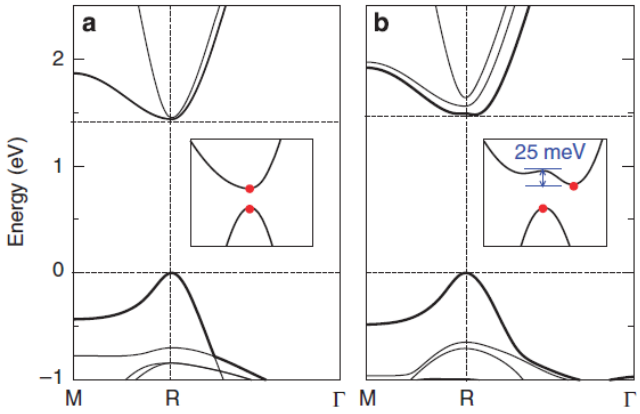

FIG. 5. Shift in $CH_3NH_3PbI_3$ bandgap due to reorientation of the MA cation from the (111) to the (011) axis. (a) Direct band gap, obtained upon an (111) orientation of the MA cation. (b) Indirect bandgap, obtained upon reorientation of the MA cation along the (011) axis, illustrated more properly in the inset. Note that the difference between the direct and indirect transitions is only 25 meV and thus of the order of K_BT at 300 K. Image adapted from ref. 36

3.2. Dynamical band gap

Another consequence of cation dynamics might be a possible influence on the perovskite band gap and charge carrier recombination dynamics.[35] By virtue of the methylammonium cation orienting with certain crystallographic directions, the conduction band minimum can rearrange towards different symmetry points in k-space, leading to an indirect band gap. These findings were obtained using DFT, by allowing the methylammonium cation to orient along different, lower symmetry axes.[36] The change in band structure is due to the MA cation exerting strain on the PbI_6 octahedra, changing the electronic structure and thus the nature of the band gap. A zoom-in on the $CH_3NH_3PbI_3$ band gap upon MA orientation along the (111) and (011) axes is given in Fig. 5. The change towards indirect band gap behavior under small strain is a very unique feature in semiconductors. Ultimately, this dynamical band gap behavior might allow for higher conversion efficiency of $CH_3NH_3PbI_3$. This effect originates from the small difference in energy between the direct- and indirect transitions. When this difference is in the order of several K_BT, the charge carrier recombination is significantly lowered due to the presence of the indirect transition, while retaining a strong absorption rate. This leads to an increased carrier lifetime (possibly orders of magnitude), improving the photovoltaic .[36–38] Alternatively, the observed dynamical bandgap effects might also be due to momentum-dependent spin band splitting in (semi-)2D systems due to the Rashba effect.[36,39,40]

3.3. Ferroelectricity

Besides direct influence of the orientation of the methylammonium cation on the electrical and op-

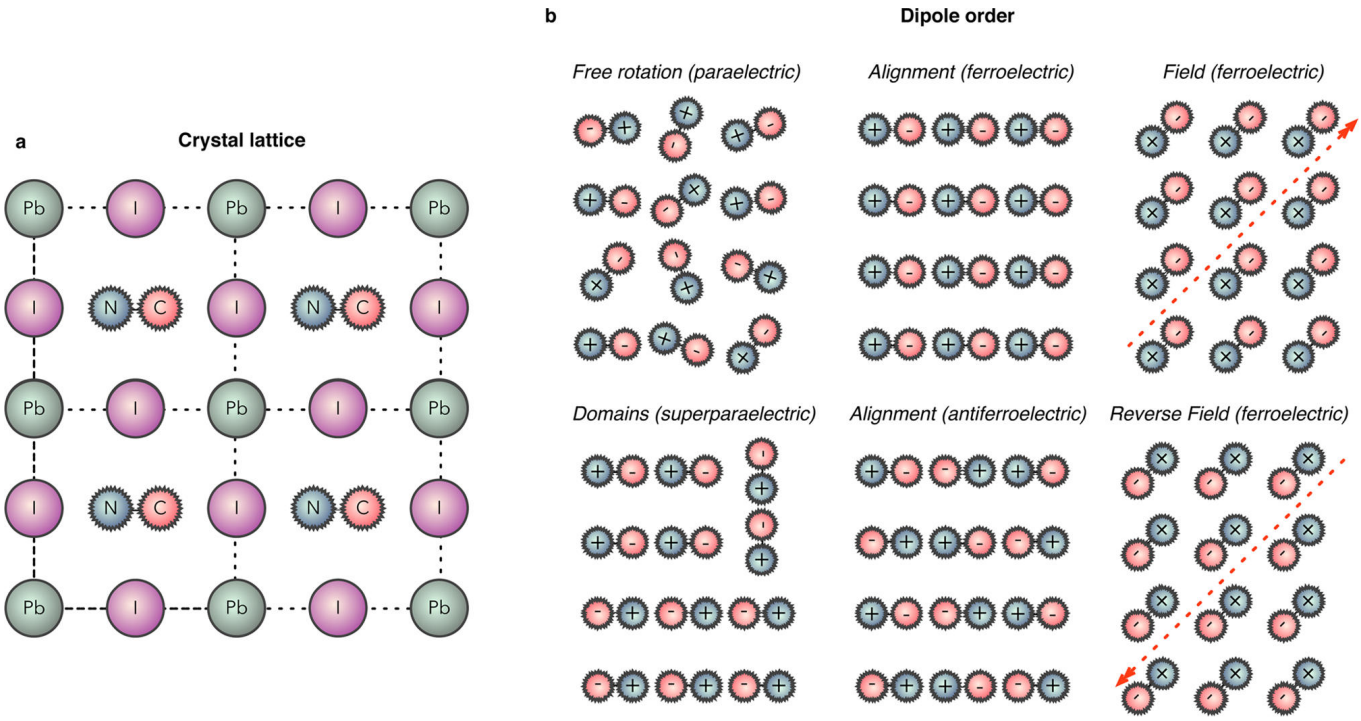

FIG. 6. Overview of ferroelectric orientations in $CH_3NH_3PbI_3$. (A) 2-dimensional cut-through of $CH_3NH_3PbI_3$. (b) Six types of possible molecular dipole orientations for the methylammonium ion in the perovskite cage. This molecular dipole is absent in fully inorganic perovskites, due to the symmetry of inorganic cations. Image adapted from ref. 8

tical properties of $CH_3NH_3PbI_3$, another possible mechanism for increased photovoltaic performance is ferroelectricity.[3,7,8,41] The definition of ferroelectricity is given as the capability of the material to have a switchable macroscopic polarization.[42] Ferroelectricity has previously been observed in oxide-based perovskites,[7,8,42,43] leading to the suggestion that it might be possible that macroscopic ferroelectric behavior could prove to play a role in hybrid perovskite photovoltaic performance as well.[3,7,8,44]

Before we discuss the macroscopic effect of ferroelectriciy on charge transport properties that might contribute to photovoltaic device performance, we need to introduce the atomistic origin of ferroelectricity in $CH_3NH_3PbI_3$. Returning to the definition of ferroelectricity, one should look for dynamics of the methylammonium cation and the perovskite cage structure that break the crystal's inversion symmetry.[7,8,45] The orientation of the methylammonium cation, the shift of the methyalammonium cation with respect to the inorganic cage structure, and the displacement of lead atoms are three options for breaking the inversion symmetry of the perovskite, allowing for a switchable polarization. These three factors are also often used in calculating the ferroelectric polarization.[7,44] The various orientations of the methyalammonium cation in $CH_3NH_3PbI_3$ that give rise to various ferroelectric or paralectric orientations are given in Fig. 6.

From a modeling point of view, ferroelectricity is treated using a semi-classical point dipole model[8] as a starting point. As an example we take the model of Frost et al.,[8] in which the equilibrium ferroelectric configuration is determined for a 2D system by building a Hamiltonian comprised of a dipole-dipole interaction term, an interaction term between the applied field E_0 and the dipoles, and a term due to local straining of the perovskite cage:

$$\hat{H} = \sum_{\mu,E}^{n}(p_i \cdot E_0) + \sum_{\mu,\mu}^{n,m} \frac{1}{4\pi\epsilon_0}\left(\frac{p_i \cdot p_j}{r^3} - \frac{3(\hat{n}\cdot p_i)(\hat{n}\cdot p_j)}{r^3}\right) + \sum_{\mu,K}^{n} K\cdot(p_i \cdot \hat{x} + p_i \cdot \hat{y})\,. \quad (5)$$

In this expression, the dipoles are indicated by $p_{i,j}$, cage strain is defined as K, and a unit vector $\hat{n}$ is defined parallel to the vector r between respective dipoles. The lattice vectors coincide with the cartesian coordinates $\hat{x}$ and $\hat{y}$.[8] The above example and various other studies[1,44] all indicate the possibility of ferroelectric domain formation at room temperature.

Based on ferroelectric domain formation in $CH_3NH_3PbI_3$, we can now focus on the macroscopic consequences of ferroelectricity in hybrid perovskites. Two mechanisms can be identified that could contribute to the extraordinary device performance of $CH_3NH_3PbI_3$-based photovoltaics.[3,7,44] These are i) enhanced charge separation and carrier lifetimes, and ii) the presence of an open circuit voltage V_{OC}, that is higher than the bandgap of the material. The latter is also denoted as the bulk photovoltaic effect.[46]

Increased charge separation is a consequence of ferroelectric domain formation, for which Frost et al.[7] have proposed a working mechanism: Namely, the presence of ferroelectric domains acting as a collection of p-n junctions, leading to what has been labeled in literature a 'ferroelectric highway'.[1,3,7] An illustration of this concept is given in Fig. 7

In traditional photovoltaics, charge separation occurs via the well-known p-n junction. In a ferroelectric domain, the equivalent is achieved by separation of the exciton that is created by photoabsorption.[7] Whereas charge carriers in conventional semiconductors have to diffuse through the relatively large (μm) junction, the nanometer sized ferroelectric domains allow for a relatively easy diffusion of carriers to the domain boundaries. Relative minima-or maxima of the built-in potential can be found at these domain boundaries, based on the relative alignment of the neighbouring ferroelectric domains that comprise these boundaries. The electrons (holes) then diffuse via the according minima (maxima) towards the respective electrodes. As of current, this is the mechanism that is proposed for explaining the high diffusion lengths in perovskites. This finding is supported by work from Sherkar et al.,[1] who used a macroscopic drift-diffusion models to show that charge transport via domain walls occurs in highly ordered ferroelectric materials.

The second mechanism that contributes to increased charge transfer properties in hybrid perovskites could be the occurence of the bulk photovoltaic effect.[3,7,46] In oxide-based perovskites, this phenomenon has been previously observed, using shift currents as a mechanism.[45] The shift current effect, which forms the basis for the bulk photovoltaic effect, can be explained in terms of broken symmetries in the $CH_3NH_3PbI_3$ crystal. As was shown in earlier sections, the orientation of the methylammonium influences the strain on the PbI_6 octahedrals in the perovskite crystal structure, breaking its inversion symmetry. Photoexcitation in the non-centrosymmetric distorted $CH_3NH_3PbI_3$ cages allows for non-linear effects, manifesting in a coherent superposition of excited states[45]. The important difference between centrosymmetric and non-centrosymmetric crystals in this regard is the following: upon photoexcitation in conventional centrosymmetric crystals, the probability of charge carriers to make the transition between a state with momentum $\mathbf{k}'$ to a state with momentum $\mathbf{k}$ is the same as for the reverse transition. In non-centrosymmetric crystals, these probabilities are not the same, leading to an asymmetric momentum distribution for excited charge carriers.[47] The asymmetric momentum distribution results in a photovoltaic current J that has a preferred direction, and is not limited by the band gap. Shift currents are a mechanism of the bulk photovoltaic effect in ferroelectric oxide materials, allowing for higher open circuit voltages than the material's bandgap and an increased carrier diffusion

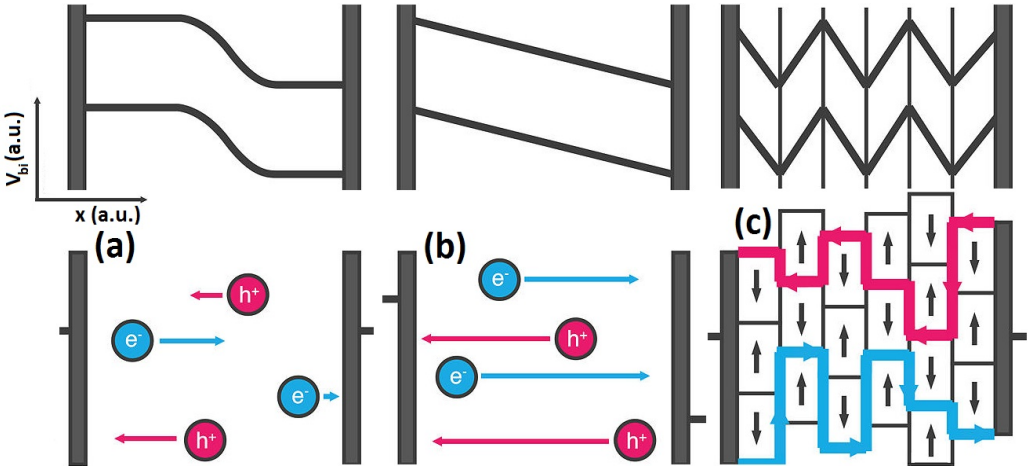

FIG. 7. Schematic depiction of the built-in potential and the corresponding charge separation. (a): Built-in potential for an n-p junction (upper) and corresponding electron- and hole separation (lower). (b): Built-in potential (upper) and charge separation (lower) within a single polarized ferroelectric domain. (c): Built-in potential (upper) for ferroelectric domains having alternating polarizations, with corresponding charge transport via domain edges (lower). The electrons (holes) move along minima (maxima) in the potential landscape. Image adapted from ref. 7

length.[48] These two properties are potentially beneficial for device performance. Using DFT, Zheng et al.[46] reported shift currents three times larger than those observed in typical ferroelectric materials. Provided that the methylammonium molecules' dipole moments were ferroelectrically aligned in parallel, significantly higher shift currents were obtained as compared to antiparallel domain orientations. This leads to the suggestion that the presence of the dipole originating from the methylammonium cation can possibly influence the $CH_3NH_3PbI_3$ device performance via the shift current mechanism.

3.4. Defect physics and device performance

A different atomistic contribution to the high performance parameters of perovskite devices could be the rather unique defect physics of $CH_3NH_3PbI_3$. In conventional semiconductors, the presence of defects in the form of doping can be a key factor in device performance, with shallow defect states allowing for increased conductance. However, deep energy level defects can act as non-radiative Shockley-Read-Hall recombination centers and carrier traps, reducing photovoltaic device performance.[3] Yin et al.[23] performed DFT calculations on defect formation energies in $CH_3NH_3PbI_3$, using three types of chemical potentials: p-type (I-rich, Pb-poor), intrinsic and n-type (I-poor, Pb-rich). The meaning of these three potentials consists of the relative chemical potentials of the CH_3NH_3 or Pb sources, as used during the growth of α-phase $CH_3NH_3PbI_3$. Considering all types of point defects (vacancies V_i, interstitials $CH_3NH_{3,i}$, Pb_i and I_i, cation substitutions between CH_3NH_3 and Pb, and substitutions between CH_3NH_3 or Pb and I), the corresponding formation energies were calculated. An overview the various intrinsic point defect formation energies as a function of Fermi level for the three different chemical potentials is given in Fig. 8a-c. The grey lines in Fig. 8a-c denote defects with high formation energy, which are unlikely to occur during perovskite crystal growth.[3,23]. One can define transition energy levels for the various defects as the Fermi level position where the defect can donate or accept electrons. The transition energy levels for the various calculated defects are depicted in Fig. 8d and e. The high formation energies in Fig. 8a-c correspond tot the deep-bandgap defects depicted in Fig. 8d and e. Therefore, deep-bandgap defect states are unlikely to occur in perovskite materials, yielding an absence of Shockley-Read-Hall recombination centers. This given

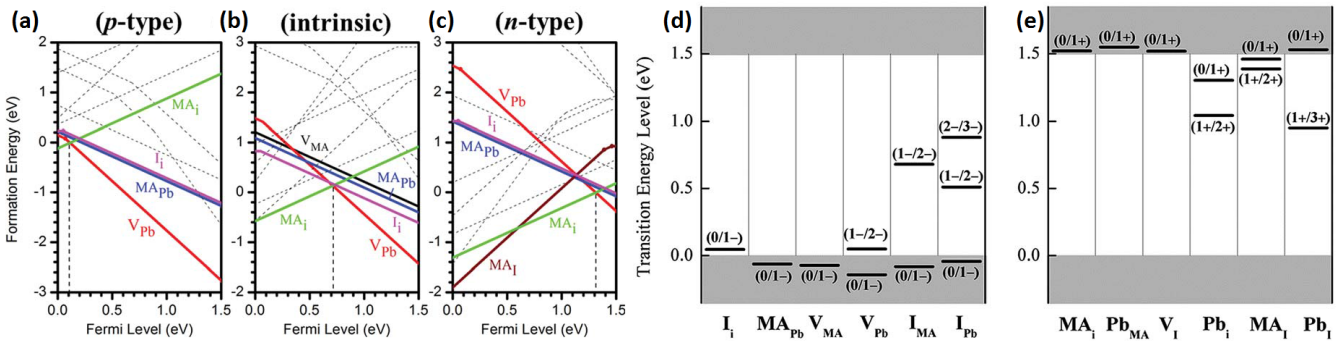

FIG. 8. Intrinsic point defect formation- and transition energies for $CH_3NH_3PbI_3$. (a-c) Overview of defect formation energies under equilibrium $CH_3NH_3PbI_3$ crystal growth for various chemical potentials (I-rich (a), intrinsic (b) and Pb-rich (c)), as a function of Fermi energy. The grey dotted lines indicate high formation energy defects, which in practice do not occur. (d) Transition energy levels for intrinsic defect acceptor levels in $CH_3NH_3PbI_3$. (e) Transition energy levels for intrinsic defect donor levels in $CH_3NH_3PbI_3$. Images adapted from refs. 3 and 23

allows for the large recombination length in perovskite materials, and contributes to the reported high device performance.[3,23] Comparable findings were obtained using DFT calculations for the β-phase of $CH_3NH_3PbI_3$ by considering Frenkel defects and Schottky defects.[18,49]

The absence of deep-band gap trapping states and the presence of only shallow defect states can be coupled to the ionic interplay between $CH_3NH_3^+$ and the perovskite cage. As mentioned in section 1.2, $CH_3NH_3PbI_3$ possesses an inverted band structure.[3,4,15] The dominant defect features in Fig. 8 consist of acceptors V_{Pb} MA_{Pb} and donors MA_i and V_I. The acceptor states are shallow due to coupling between the Pb s lone pair and the I p orbital, which pushes the states to an antibonding state near the valence band maximum. A high ionicity is present between methylammonium and Pb, with only a small covalent contribution via the Pb p orbital. This again, yields states very close to the conduction band minimum.[3,15,23,50]

4. VALIDITY OF THEORETICAL MODELS

So far, three atomistic origins of hybrid perovskite performance have been discussed. These consist of i) the effects of the preferred orientations and vibrational dynamics of the dipolar organic cation on the band gap character, ii) the large scale ferroelectric consequences of dipoles in $CH_3NH_3PbI_3$, consisting of ferroelectric highways and the bulk photovoltaic effect, and iii) increased charge carrier transport due to extraordinary defect physics. In order to critically assess the feasibility of these three mechanisms, discussion of the underlying physical assumptions and a revision of computational limitations is necessary. Regardless of the feasibility of these models, it is apparent from the diversity of the discussed models that the performance of hybrid perovskite photovoltaics cannot be attributed to a single mechanism, but is rather a combination of multiple physical effects that separate it from conventional materials such as GaAs.

4.1. Model assumptions: limitations, scaling and temperature

A first remark is in place about the computational limitations that were made in section 2.1. A persistent problem in the application of *ab initio* models in simulating various perovskite properties is that as of now, only a limited number of atoms can be modelled at the same time, for a limited timescale. To put this statement in context, we note that the studies on the dynamical band gap,[35,36] defect physics[23] and ferroelectricity[7,8,44] all use the same method for circumventing this problem. All studies try

to solve this apparent scaling problem by performing *ab initio* calculations on $CH_3NH_3PbI_3$ supercells, consisting of various repeats of the perovskite unit cell, such that ultimately only several tens of atoms are simulated at once. Periodic boundary conditions are then applied, in order to extend the physics of the several simulated unit cells is extended to a macroscopically sized system. The application of periodic boundary conditions is necessary in DFT calculations.[44] Alternatively, the ferroelectric study by Frost et al.[8] even goes as far as to treat the ferroelectric lattice as a 2-dimensional system. Also, for all methods that extend the simulated region to bulk properties, the short simulation times (< 100 ps) are not improved.

Based on the extension of supercell properties to macroscopic properties, one might raise the question on whether calculations of ferroelectric polarization are feasible when periodic boundary conditions or a lower dimensionality of the system are assumed. One simple argument in this regard is that the dipolar interaction, or structural disorder takes place on a length scale comparable to- or larger than the modeled super cells.

Another point that is worth mentioning with regards to the scaling of the modeled physics, is that macroscopic models possibly ignore the relation with the specific dynamics of the organic perovskite cation. An example is the 3D drift-diffusion model used by Sherkar et al.[1] This specific study yielded a quantitative understanding of perovskite performance in terms of charge transport channels via ferroelectric domains. Also, by picking a sufficiently low recombination strength of the charge carriers (γ_{pre}=10^{-4}), effective charge separation was achieved. The caveat with this method is however that it fails to include the real atomistic origin and thus the cation dynamics into its description of device performance. Also, the large domain size is, as the authors justifiably notice, not realistic.

4.2. Thermal effects: real and ideal

Besides the question whether the properties simulated on small supercells scale properly to the simulated bulk properties, there are is another key parameter that requires attention: temperature. Also, the assumptions that were made in the presented studies regarding temperature partly reside in computational arguments.

First we need to mention the fact that the room-temperature β-phase of $CH_3NH_3PbI_3$ is the key phase to describe with respect to device performance. It is striking then, that various studies[36,44] provide DFT calculations at 0 K for the β-phase (correspondingly also for the α-phase[23]), whereas these phases do not exist at this temperature. Based on calculations of ferroelectric polarization at 0 K in oxide-based ferroelectric perovskites[44,51,52] and the fact that DFT *de facto* does not take into account any dynamics, the discrepancy between DFT temperatures and the modeled crystal phases does not seem to be problematic. However, low temperature approximations can prove to be problematic. *Ab initio* calculations from Carignano et al.[28] indicate that properties correlated to the dynamical structure of both the organic cation and the inorganic perovskite cage can be strongly influenced by thermal- and finite size effects. Their calculations are based on placing no spatial constraints on the position of the atoms in $CH_3NH_3PbI_3$. Their results indicate that when using a $2\times2\times2$ $CH_3NH_3PbI_3$ supercell, the dynamics of the methylammonium cation cannot be decoupled from neighbouring supercells. This indicates that the dynamics of the cation are heavily influenced by the size of the simulated supercell, which is conflicting with nearly all of the presented theoretical results, which used repeating supercells.[5,23,36,44] They also found that the modeled structures experience heavy thermal fluctuations during the first several picoseconds of the simulation runtime.

It is clear from the reviewed theoretical work that the modeling of perovskites is a problem consisting of multiple variables. The inconsistency of the physical assump-

tions across multiple studies[7,8,23,36,44] and the requirement of macroscopic models[1] for providing a quantitative analysis together call for a so-called multi-scale modeling approach. The relation between cation dynamics and macroscopic device parameters can simply not be fully solved by a plethora of different models treating different variables based on different assumptions. Some areas of physics, i.e. solid mechanics, have already succesfully embraced multi-scale methods.[53] The advent of multiscale modeling for photovoltaics might however be far away, considering the current computational limitations.

5. RELATION THEORY AND EXPERIMENT

Besides an assessment of the physical feasibility of the discussed theoretical models, it is also necessary to perform a reality check with respect to the degree in which the predictions match experimental results. This analysis can be divided in a discussion on the relation between real crystal structures and defects on the predicted $CH_3NH_3PbI_3$ properties, and experimental observations of possible ferroelectricity in $CH_3NH_3PbI_3$.

5.1. Structural variations

As was mentioned in section 1.1, a treatment of crystal structures is not complete without considering the formation of grains. Therefore, it is necessary to compare the assumed crystal structures in band structure- and defect state calculations to observed crystal structures, such that we can attest the feasibility of the former.

None of the cited works on dynamical band gap behavior,[36] ferroelectricity[1,7,8,44] or defect physics[23] managed to incorporate the formation of crystallographic domains in the β-phase. As mentioned in section 1.1, a lower symmetry phase, with grains on the scale of several lattice constants (1.4 nm) was observed using X-ray diffraction and should be included in the calculation of these properties.[14]

In the discussed studies on defect physics and charge trapping states, Yin et al.[15] assume a perfect α-phase perovskite. Principally, we can identify two problems with this approach. First is obviously the fact that polycrystalline domains are not taken in consideration. Second is the fact that as for other studies, the α-phase does not coincide with the room-temperature β-phase. The same Yin in later studies on CdTe photovoltaics show that the presence of grain boundaries lead to deep-band gap defect states, reducing photovoltaic performance.[54]

Likewise, Motta et al.[36] perform exactly the same assumptions, and base their prediction of dynamical band gap behavior on the strain exerted by the methylammonium cation on the perovskite cage in certain orientations. It should however be clear that for this study the same argument holds: the presence of grains could lead to a completely different band structure.

Whereas most studies fail to include the presence of the lower crystal symmetry due to crystal grains, the question remains whether the influence of grain formation is large enough to actually be considered in theoretical calculations. Bakulin et al.[5] showed using anisotropy decay in 2D-IR experiments that the reorientation dynamics of the methylammonium cation in $CH_3NH_3PbI_3$ seem insensitive to different types of crystallographic domains. They based this result on clear agreement between decay trends obtained from $CH_3NH_3PbI_3$ samples that were fabricated using different methods. The anisotropy decay data for three thin-film preparation methods, including fits, are displayed in Fig. 9.

Also, Yin et al.[3] again return to their work on defects and show that the effect of grain boundaries on electronic structure is in all likeliness small. They argue that the effect of grain boundaries in polycrystalline $CH_3NH_3PbI_3$ is small on basis of two arguments. First, they assume the major influence of grain boundaries to be the wrong-bonding of the I atoms. Based on the inverted band structure and strong s-p coupling in $CH_3NH_3PbI_3$ (see section 1.2), they argue that the high VBM nevertheless

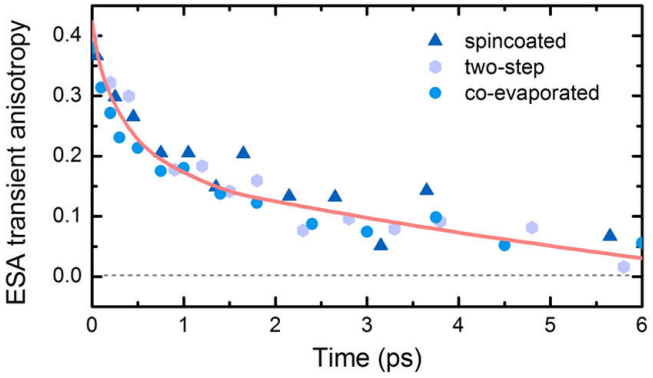

FIG. 9. Anisotropy decay with time-dependent fit, used to determine the timescale of cation dynamics in $CH_3NH_3PbI_3$ for different thin-film preparation methods. All deposition methods should result in different types of polycrystalline $CH_3NH_3PbI_3$. A qualitative agreement can be seen between the three decays, indicating that the dynamics of the methylammonium cation are insensitive to the formation of crystal grains and corresponding grain boundaries. Image adapted from ref. 5

will lead to low-lying defect levels due to grain boundaries. They support this notion by mentioning that the I-I bond length is relatively large as compared to the deep-bandgap grain boundary defect levels in other solar cell absorbers, making the I-I interaction weak.

Based on the experimental results from Bakulin et al.,[5], and the reasoning of Yin et al.,[3] we can conclude that the lack of involvement of grain effects in the discussed theoretical works can be justified. Besides the fact that these results indicate that grain boundaries do not negatively influence $CH_3NH_3PbI_3$ device performance, we should also note that recent developments in perovskite device fabrication might make this discussion obsolete. Recently, perovskite crystal grains as large as a single millimeter have been fabricated with low defect levels, indicating that perovskite photovoltaics might soon evolve beyond the point of grain boundaries posing a significant problem in theoretical- and experimental treatments.[55–57]

5.2. Ferroelectric observations

Two of the possible mechanisms via which ferroelectricity contributes to $CH_3NH_3PbI_3$ device performance are the presence of a ferroelectric highway and a possible contribution to the bulk photovoltaic effect via the shift current mechanism.[7,46] Both mechanisms are based on the presence of a macroscopic polarization due to ferroelectric domain formation at room temperature.

One experimental feature of perovskite devices that has often been linked to the presence of ferroelectric domains is current/voltage (J-V) hysteresis.[2,58] This reversible hysteresis can be observed during device efficiency (photocurrent-voltage) measurements.[30] Namely, an asymmetry was observed when sweeping the voltage over the device back and forth between a forward bias and V_{OC}, with photocurrents taking tens of seconds to stabilize.[58] One can thus try to prove the presence of ferroelectric domains indirectly by matching the reported J-V hystereses, and according polarization-electric field (P-E) hysteresis. Experimental observations however, seem to suggest that ferroelectric domain switching has very little to do with the observed hysteresis.[30,44,60] Leguy et al.[30] provide an upper bound in the millisecond range to the J-V hysteresis time, if the hysteresis would be due to ferroelectric domain switching. This is several orders of magnitude lower than the observed J-V hysteresis timescale,[2] and thus indicative of ferroelectricity not playing a role. Similarly, P-E hysteresis measurements by Fan et al.[44] dispel the possibility of ferroelectric domain switching to contribute to the observed hysteresis. It could well be possible that the presence of J-V and/or P-E hysteresis is largely due to the trapping of charges near the TiO_2 layer in perovskite devices, or due to the migration of ionic defects.[58,61,62]

Alternatively, attempts have also been made to directly observe room-temperature ferroelectric domains in $CH_3NH_3PbI_3$ via piezoresponse force microscopy (PFM).[44,59] A certain discrepancy exists between differ-

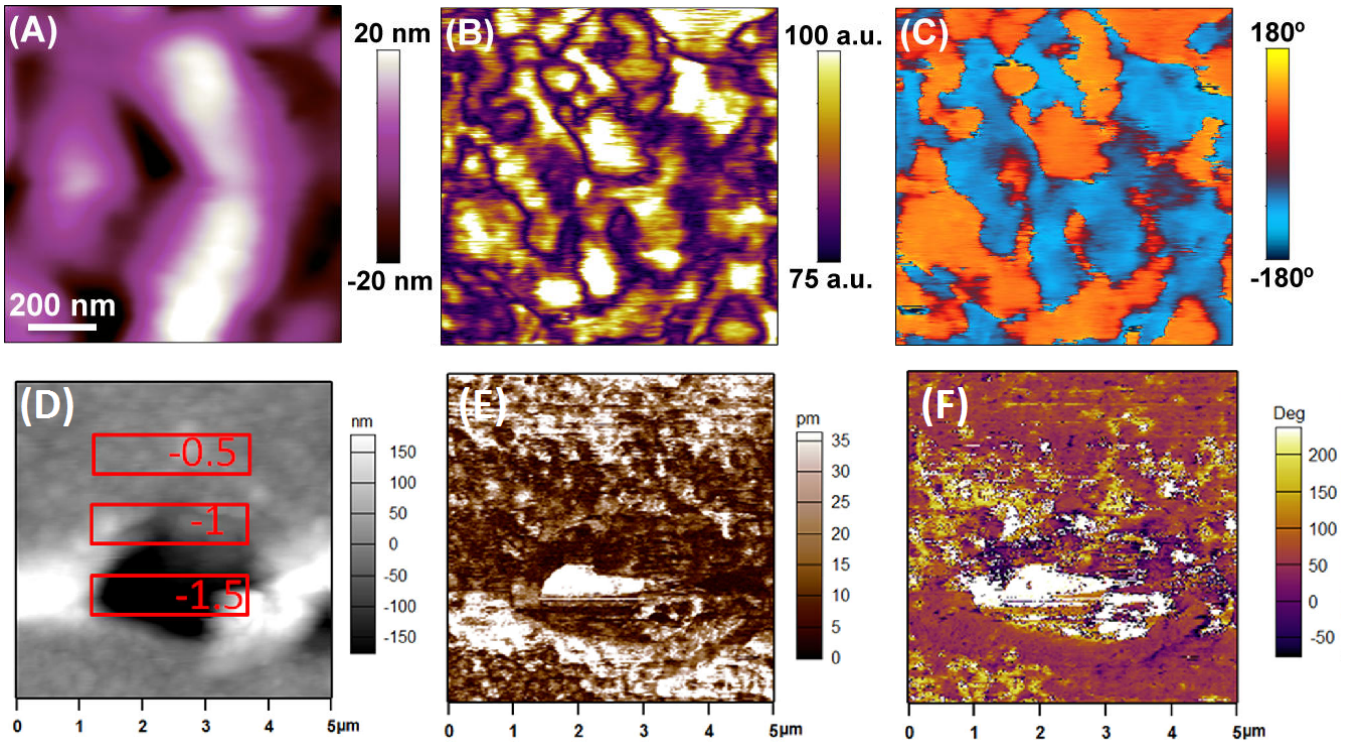

FIG. 10. Comparison of piezoresponse force microscopy (PFM) results on $CH_3NH_3PbI_3$ between Kutes et al. (a-c) and Fan et al. (d-f). (a) 1×1 μm AFM topography image. (b) PFM amplitude. (c) PFM phase. Kutes et al. report that the observed domains were switchable under opposite tip bias. The ferroelectric domain size and the average grain size are approximately the same. (d) 5×5 μm AFM topography image, with red boxes indicating the poled regions and corresponding tip voltages. (e) PFM amplitude. (f) PFM phase. In the images from fan et al, a correlation between the strongly negatively poled region in the topography image and the corresponding PFM amplitude and phase images is visible. The authors indicate that the contrast is not due to ferroelectricity, but instead due to surface electrochemistry. Images adapted from refs. 44 and 59

ent PFM-based results, as well as the theoretical predictions. Kutes et al.[59] claim to have observed ferroelectric domains in β-phase $CH_3NH_3PbI_3$ using PFM, having observed switchable ferroelectric domains of approximately 100 nm in size (Fig. 10a-c). However, the correspondence between topography (grain size) and ferroelectric domain size is at least striking. Furthermore, Fan et al.[44] report no observation of ferroelectric domains using PFM under the same ambient conditions and usage of PFM tip poling. They report any contrast, occurring at relatively high negative tip voltages, to electrochemical effects instead of ferroelectric domain switching (Fig. 10d-f). The observations made by Fan et al. are further supported by comparable findings from Xiao et al.[63]

Whereas the theoretical work by Frost[7], Zheng[46] and Sherkar[1] indicate the possiblity of ferroelectricity contributing to macroscopic charge properties, experimental work[44,59,63] has thus far failed to catch up in a consistent manner. The safe conclusion for now is thus that whereas ferroelectricity is a likely candidate to play *some* role in the performance of perovskites via several mechanisms, no exact mechanism can be pinpointed due to the lack of experimental confirmation of its existence. Whether the computational assumptions and finite size effects mentioned in section 4.1 could have led to overstated manifestations of ferroelectricity remains to be investigated.

6. CONCLUSIONS

A sound theoretical understanding of the working mechanisms behind the extraordinary device performance of hybrid perovskite photovoltaics, with an em-

phasis on $CH_3NH_3PbI_3$, is necessary in order to fast-track developments and possible implementation of this technology. In this review, we have discussed various mechanisms contributing to improved device performance, specifically from the perspective of methylammonium cation dynamics. These mechanisms consist of i) the contribution of the methylammonium cation orientation to indirect band gap behavior, ii) ferroelectricity and a resulting ferroelectric highway, and bulk photovoltaic effect via shift currents and iii) lack of deep bandgap charge trapping states due to the interplay between the methylammonium cation and the inverted semiconductor band structure in $CH_3NH_3PbI_3$. In order to assess these findings, which were all based on different *ab initio* models, we investigated the presented theoretical works from two viewpoints. First, we assessed the computational limitations and physical assumptions, as well as the relation between real- and assumed crystal structures. From this analysis, we found that many theoretical studies of perovskite properties suffer from finite size effects, meaning that the relationship between the microscopic cation properties and the macroscopic charge transport properties of the perovskites is not specifically trustworthy. This argument holds for both the dynamical band gap mechanism as ferroelectricity. We also found that the occurrence of grain boundaries, and their lack of implementation in physical models did not prove problematic from both a principal point of view as well as an experimental point of view.

Furthermore, we also compared recent experimental works on J-V hysteresis and ferroelectric domain formation, in order to assess whether the predicted ferroelectricity at ambient conditions is a feasible mechanism for explaining perovskite photovoltaic behavior. We found inconsistencies between PFM-, J-V hysteresis, neutron scattering measurements and the theoretical predictions on domain size and hysteresis properties of ferroelectric $CH_3NH_3PbI_3$. From this discrepancy, we conclude that, based on the earlier discussion of finite size effects, it is for now unlikely that ferroelectricity plays a very significant role in perovskite photovoltaic performance.

Ultimately, we conclude that the relationship between cation dynamics and the performance of hybrid perovskite photovoltaics is a problem of many variables, as the cation dynamics play a role via various mechanisms, occurring at varying length scales. The methodological inconsistencies amongst most of the theoretical studies and the influence of finite size effects call for a multi-scale approach for tackling the hybrid perovskite working mechanisms. The same philosophy applies for the experimental work that we took as a comparison: also here there prove to be many inconsistencies between both microscopic measurements (PFM) and macroscopically scaled properties (J-V hysteresis). These conclusions illustrate in a broad sense the biggest challenge in the field of nanoscience: to couple the microscopic to macroscopic properties in both a theoretical and experimental way.

[1] T. S. Sherkar and L. J. A. Koster, Physical Chemistry Chemical Physics **18**, 331 (2015).

[2] H. J. Snaith, The Journal of Physical Chemistry Letters **4**, 3623 (2013).

[3] W.-J. Yin, J.-H. Yang, J. Kang, Y. Yan, and S.-H. Wei, Journal of Materials Chemistry A **3**, 8926 (2015).

[4] M. A. Green, A. Ho-Baillie, and H. J. Snaith, Nature Photonics **8**, 506 (2014).

[5] A. A. Bakulin, O. Selig, H. J. Bakker, Y. L. Rezus, C. Müller, T. Glaser, R. Lovrincic, Z. Sun, Z. Chen, A. Walsh, J. M. Frost, and T. L. C. Jansen, The Journal of Physical Chemistry Letters **6**, 3663 (2015).

[6] N. Onoda-Yamamuro, T. Matsuo, and H. Suga, Journal of Physics and Chemistry of Solids **53**, 935 (1992).

[7] J. M. Frost, K. T. Butler, F. Brivio, C. H. Hendon, M. van Schilfgaarde, and A. Walsh, Nano Letters **14**, 2584 (2014).

[8] J. M. Frost, K. T. Butler, and A. Walsh, APL Materials **2**, 081506 (2014).

[9] N. Pellet, P. Gao, G. Gregori, T.-Y. Yang, M. K. Nazeeruddin, J. Maier, and M. Grätzel, Angewandte Chemie International Edition **53**, 3151 (2014).

[10] C. C. Stoumpos, C. D. Malliakas, and M. G. Kanatzidis, Inorganic Chemistry **52**, 9019 (2013).

[11] W.-J. Yin, Y. Yan, and S.-H. Wei, The journal of physical chemistry letters **5**, 3625 (2014).

[12] T. Baikie, Y. Fang, J. M. Kadro, M. Schreyer, F. Wei, S. G. Mhaisalkar, M. Graetzel, and T. J. White, Journal of Materials Chemistry A **1**, 5628 (2013).

[13] S. Colella, E. Mosconi, P. Fedeli, A. Listorti, F. Gazza, F. Orlandi, P. Ferro, T. Besagni, A. Rizzo, G. Calestani, *et al.*, Chemistry of Materials **25**, 4613 (2013).

[14] J. J. Choi, X. Yang, Z. M. Norman, S. J. L. Billinge, and J. S. Owen, Nano Letters **14**, 127 (2014).

[15] W.-J. Yin, T. Shi, and Y. Yan, Advanced Materials **26**, 4653 (2014).

[16] I. Borriello, G. Cantele, and D. Ninno, Physical Review B **77**, 235214 (2008).

[17] F. Brivio, A. B. Walker, and A. Walsh, APL Materials **1**, 042111 (2013).

[18] M. H. Du, Journal of Materials Chemistry A **2**, 9091 (2014).

[19] L. Lang, J.-H. Yang, H.-R. Liu, H. J. Xiang, and X. G. Gong, Physics Letters A **378**, 290 (2014).

[20] G. Giorgi, J.-I. Fujisawa, H. Segawa, and K. Yamashita, The Journal of Physical Chemistry Letters **4**, 4213 (2013).

[21] L. Yu, R. S. Kokenyesi, D. A. Keszler, and A. Zunger, Advanced Energy Materials **3**, 43 (2013).

[22] L. Yu and A. Zunger, Physical Review Letters **108**, 068701 (2012).

[23] W.-J. Yin, T. Shi, and Y. Yan, Applied Physics Letters **104**, 063903 (2014).

[24] D. Marx and J. Hutter, Modern methods and algorithms of quantum chemistry **1**, 141 (2000).

[25] W. Kohn and L. J. Sham, Physical review **140**, A1133 (1965).

[26] R. Car and M. Parrinello, Physical Review Letters **55**, 2471 (1985).

[27] D. K. Remler and P. A. Madden, Molecular Physics **70**, 921 (1990).

[28] M. A. Carignano, A. Kachmar, and J. Hutter, The Journal of Physical Chemistry C **119**, 8991 (2015).

[29] R. E. Wasylishen, O. Knop, and J. B. Macdonald, Solid State Communications **56**, 581 (1985).

[30] A. M. A. Leguy, J. M. Frost, A. P. McMahon, V. G. Sakai, W. Kockelmann, C. Law, X. Li, F. Foglia, A. Walsh, B. C. ORegan, J. Nelson, J. T. Cabral, and P. R. F. Barnes, Nature Communications **6**, 7124 (2015).

[31] V. F. Sears, Neutron news **3**, 26 (1992).

[32] P. Hamm, M. Lim, and R. M. Hochstrasser, The Journal of Physical Chemistry B **102**, 6123 (1998).

[33] P. Hamm and M. Zanni, *Concepts and methods of 2D infrared spectroscopy* (Cambridge University Press, 2011).

[34] T. l. C. Jansen and J. Knoester, Accounts of Chemical Research **42**, 1405 (2009).

[35] E. Mosconi, A. Amat, M. K. Nazeeruddin, M. Grätzel, and F. De Angelis, The Journal of Physical Chemistry C **117**, 13902 (2013).

[36] C. Motta, F. El-Mellouhi, S. Kais, N. Tabet, F. Alharbi, and S. Sanvito, Nature Communications **6**, 7026 (2015).

[37] S. Fonash, *Solar cell device physics* (Elsevier, 2012).

[38] J. J. Loferski, Journal of Applied Physics **27**, 777 (1956).

[39] F. Brivio, K. T. Butler, A. Walsh, and M. van Schilfgaarde, Physical Review B **89**, 155204 (2014).

[40] A. Stroppa, D. Di Sante, P. Barone, M. Bokdam, G. Kresse, C. Franchini, M.-H. Whangbo, and S. Picozzi, Nature Communications **5**, 5900 (2014).

[41] K. T. Butler, J. M. Frost, and A. Walsh, Energy & Environmental Science **8**, 838 (2015).

[42] R. E. Cohen, Nature **358**, 136 (1992).

[43] J. Haeni, P. Irvin, W. Chang, R. Uecker, P. Reiche, Y. Li, S. Choudhury, W. Tian, M. Hawley, B. Craigo, *et al.*, Nature **430**, 758 (2004).

[44] Z. Fan, J. Xiao, K. Sun, L. Chen, Y. Hu, J. Ouyang, K. P. Ong, K. Zeng, and J. Wang, The Journal of Physical Chemistry Letters **6**, 1155 (2015).

[45] S. M. Young and A. M. Rappe, Physical review letters **109**, 116601 (2012).

[46] F. Zheng, H. Takenaka, F. Wang, N. Z. Koocher, and A. M. Rappe, The Journal of Physical Chemistry Letters **6**, 31 (2015).

[47] V. Fridkin, Crystallography Reports **46**, 654 (2001).

[48] K. Uchino, Y. Miyazawa, and S. Nomura, Japanese Jour-

nal of Applied Physics **21**, 1671 (1982).

[49] J. Kim, S.-H. Lee, J. H. Lee, and K.-H. Hong, The Journal of Physical Chemistry Letters **5**, 1312 (2014).

[50] W.-J. Yin, S.-H. Wei, M. M. Al-Jassim, and Y. Yan, Applied Physics Letters **99**, 142109 (2011).

[51] K. M. Rabe and P. Ghosez, in *Physics of ferroelectrics* (Springer, 2007) pp. 117–174.

[52] J. Neaton, C. Ederer, U. Waghmare, N. Spaldin, and K. Rabe, Physical Review B **71**, 014113 (2005).

[53] M. F. Horstemeyer, in *Practical aspects of computational chemistry* (Springer, 2009) pp. 87–135.

[54] C. Li, Y. Wu, J. Poplawsky, T. J. Pennycook, N. Paudel, W. Yin, S. J. Haigh, M. P. Oxley, A. R. Lupini, M. Al-Jassim, *et al.*, Physical review letters **112**, 156103 (2014).

[55] W. Nie, H. Tsai, R. Asadpour, J.-C. Blancon, A. J. Neukirch, G. Gupta, J. J. Crochet, M. Chhowalla, S. Tretiak, M. A. Alam, *et al.*, Science **347**, 522 (2015).

[56] D. Shi, V. Adinolfi, R. Comin, M. Yuan, E. Alarousu, A. Buin, Y. Chen, S. Hoogland, A. Rothenberger, K. Katsiev, *et al.*, Science **347**, 519 (2015).

[57] M. I. Saidaminov, A. L. Abdelhady, B. Murali, E. Alarousu, V. M. Burlakov, W. Peng, I. Dursun, L. Wang, Y. He, G. Maculan, *et al.*, Nature communications **6** (2015).

[58] H. J. Snaith, A. Abate, J. M. Ball, G. E. Eperon, T. Leijtens, N. K. Noel, S. D. Stranks, J. T.-W. Wang, K. Wojciechowski, and W. Zhang, The journal of physical chemistry letters **5**, 1511 (2014).

[59] Y. Kutes, L. Ye, Y. Zhou, S. Pang, B. D. Huey, and N. P. Padture, The Journal of Physical Chemistry Letters **5**, 3335 (2014).

[60] B. C. ORegan, P. R. Barnes, X. Li, C. Law, E. Palomares, and J. M. Marin-Beloqui, Journal of the American Chemical Society **137**, 5087 (2015).

[61] Y. Shao, Z. Xiao, C. Bi, Y. Yuan, and J. Huang, Nature communications **5** (2014).

[62] J. Beilsten-Edmands, G. E. Eperon, R. D. Johnson, H. J. Snaith, and P. G. Radaelli, Applied Physics Letters **106**, 173502 (2015).

[63] Z. Xiao, Y. Yuan, Y. Shao, Q. Wang, Q. Dong, C. Bi, P. Sharma, A. Gruverman, and J. Huang, Nature materials **14**, 193 (2015).